Automatic extraction of facial interest points based on 2D and 3D data

Nesli Erdogmus, Jean-Luc Dugelay
EURECOM, Multimedia and Communications Department, Image Processing Group
2229 Route des Crêtes, BP 193 F-06560 Sophia-Antipolis cedex
{nesli.erdogmus, jean-luc.dugelay}@eurecom.fr

ABSTRACT

Facial feature points are one of the most important clues for many computer vision applications such as face normalization, registration and model-based human face coding. Hence, automating the extraction of these points would have a wide range of usage. In this paper, we aim to detect a subset of Facial Definition Parameters (FDPs) defined in MPEG-4 automatically by utilizing both 2D and 3D face data. The main assumption in this work is that the 2D images and the corresponding 3D scans are taken for frontal faces with neutral expressions. This limitation is realistic with respect to our scenario, in which the enrollment is done in a controlled environment and the detected FDP points are to be used for the warping and animation of the enrolled faces [1] where the choice of MPEG-4 FDP is justified. For the extraction of the points, 2D, 3D data or both is used according to the distinctive information they carry in that particular facial region. As a result, total number of 29 interest points is detected. The method is tested on the neutral set of Bosphorus database that includes 105 subjects with registered 3D scans and color images.

Keywords: Facial interest points, automatic detection, multimodal

1. INTRODUCTION

Human face is certainly one of the most commonly utilized biometric traits in numerous computer vision applications. In most of these applications, the performance relies on facial feature point detection and obviously, automating the extraction of these interest points is crucial to obtain a stand-alone system that does not require user input. Today, thanks to the recent advances in 3D acquisition tools, the inadequacy of analyzing the 2D face images can be easily complemented by the shape information. 3D scans explicitly contain the surface information of the shape and can be very helpful to examine facial sub-regions for which texture does not reveal much information.

Integrating range and texture information for also face recognition is proven to be advantageous in studies like [2, 3]. On the other hand, a method for detection of anchor points using 2.5D face images is proposed in [4], in which the decision is based on local shape characteristics with parameters trained on sample scans. This approach is improved with a more robust nose tip extraction algorithm in [5] where additionally, the cornerness response from the intensity map

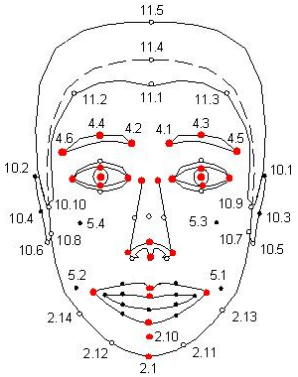

Figure 1: Facial Definition Parameters defined in MPEG-4 FA and the chosen subset to be automatically located

is utilized to determine the positions of the corners of the eyes and the mouth. This study is extended further in [6] by handling pose variance in 3D facial scans that is achieved by estimating the nose tip based on a nose profile model. In a similar way, feature points are described by Gabor filter responses in the 2D domain and point signature in the 3D domain in [8]. Another algorithm that combines 2D and 3D registered data to accurately detect the facial feature points is proposed in [7], where firstly skin regions are segmented and eye and mouth candidates are determined by processing formerly produced eye and mouth maps.

Bearing in mind that for most of the 3D acquisition systems subject cooperation is required and pose and facial expressions are well-controlled, we based our system on the assumption of frontal and neutral face images. According to our scenario proposed in [1], we need to extract a subset of MPEG-4 FDP points (Figure 1) in order to realize facial expression simulations on the enrolled models.

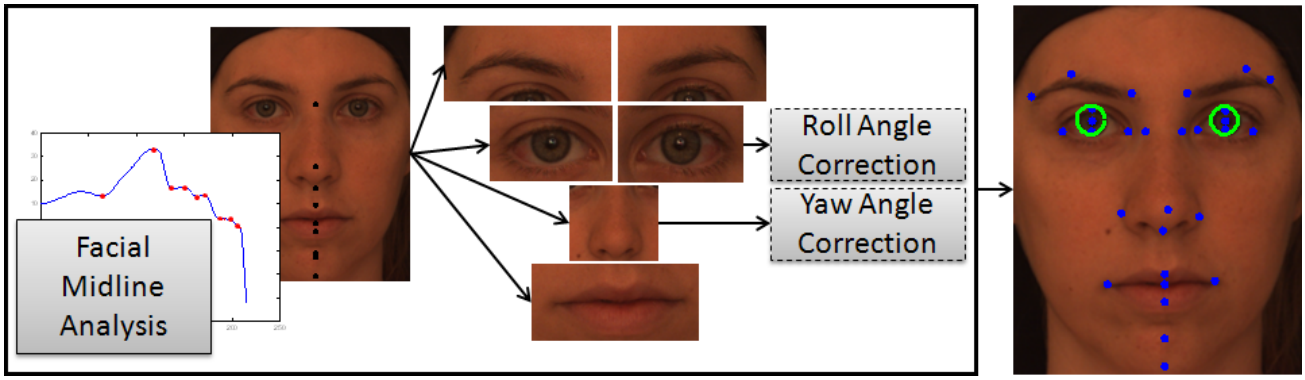

Figure 2: Flow chart for the proposed system

Firstly, facial midline (vertical profile) analysis is done and 9 fiducial points on that midline is detected. Based on that information; face is broken into sub-regions. This facilitates the coarse localization of eyebrow, eye, nose and lip. After that, further analysis is done in these extracted sub-regions to detect the points of interest. In the proposed algorithm, for those regions with non-informative texture (like nose) the 3D data is analyzed. On the other hand for the regions with noisy surface and/or distinctive color information 2D data is utilized. As a result, 29 facial interest points are detected in total, consisting of 3 points for each eyebrow, 5 points for each eye and 6 points for the nose, 5 points for the lip and finally 2 points for the chin.

The rest of this paper is organized as follows: In Section 2, vertical profile analysis and the extraction of sub-regions are explained in detail. In Section 3, methods to extract the points in each sub-region are given separately in the subsections. Finally, after the tests and results are presented in Section 4, the paper is concluded.

2. VERTICAL PROFILE ANALYSIS

The analysis done on the vertical profile constitutes the backbone of the whole system. It starts with the extraction of the facial midline and for this purpose; the method proposed in [5] is adopted. For each row, the position with the maximum z value is found and then for each column, the number of these positions is counted so that a histogram is created. The peak of this histogram is chosen as the column for the position of the vertical midline. The vertical profile is extracted and smoothed by mean filtering. This procedure is illustrated in Figure 3.

The highest point in the profile curve is detected as the nose tip. Since this knowledge of nose tip position lets us to look for the eyes in the upper half of the face, before going any further, coarse iris detection is applied in that region.

For coarse iris extraction, the non-skin region is found by removing the pixels with the most frequent (C_b, C_r) values present in the half-image, using YC_bC_r space in the 2D image. Edge maps are constructed for the non-skin region using Canny edge detector by iteratively adjusting the threshold until a descriptive edge map is obtained. Afterwards, Hough transform is applied to the edge map to detect circles. For each detected circle, an overlapping score is calculated by the ratio of the detected portion of the circle to the whole circle parameter. After grouping the detected iris candidates as right and left iris according to their positions, among the compatible pairs, the one with the maximum total overlapping score is chosen to be the two irises [9].

After the positions of the two iris centers are found, the 2D and 3D images of the face are rotated in order to align to iris centers on the same horizontal line. Thereby, our assumption for vertical profile is better assured.

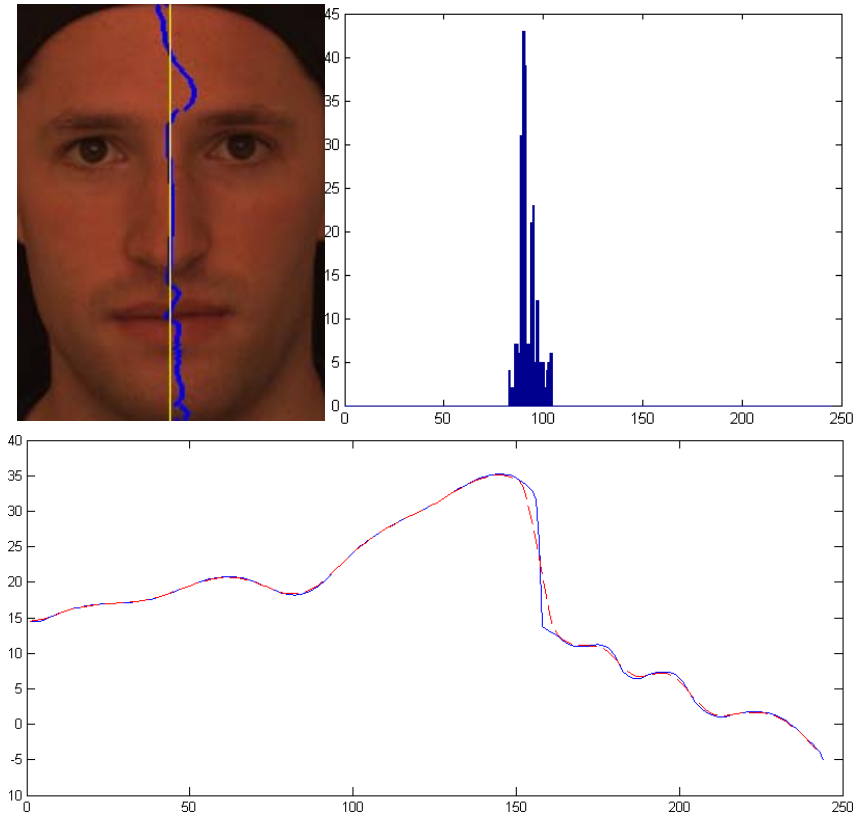

Figure 3: The positions with maximum z value for each row on the example face are marked with blue dots and the chosen column is marked with yellow. The histogram and the extracted profile before and after smoothing are given.

After correcting the roll angle of the face, the profile analysis is repeated, and this time in more detail. The vertical midline of the face is extracted and smoothed as explained before.

On a correctly extracted profile curve, there are bulges (forehead, nose, upper and lower lips and chin) and bores in between. Even though, those shapes do not fully expose the location of the facial interest points, they can be highly informative. For this reason, the peaks and nadirs in the profile curve are found with the help of the zero-crossings of the curve's first and second derivatives (differences between adjacent elements of the mid-line profile).

Firstly, the highest point on the curve is detected as nose tip and the first zero-crossing of the first derivative of the curve that is closest to the nose tip from left is labeled as the starting point and the point with the maximum second derivative value to the right of the nose tip is labeled as the end point of the nose. Afterwards, the bottom of the face is found as the point whose second derivative exceeds a threshold (0.7). Thus, three points on the nose (nose bridge, nose tip and the bottom) and the border of the chin is detected.

For the points between the end of the nose and the border of the chin, zero-crossings for both first and second derivative are calculated. Since usually, due to the spherical shape of the facial surface, this region is inclined, the "mean slope" is calculated as the difference between the end of the nose and the bottom of the face. Assuming that slope of the curve in that region is biased as that mean value, another set of "zero-crossings" are calculated by subtracting the calculated mean slope from the first derivatives.

The bulges and bores are created by the subsequent increase and decrease in the profile curve so each peak (or nadir) is bounded by two zero-crossings of the second derivative. Considering this fact, an interest point is detected as the zero-crossing of the first derivative between two "boundaries" if it exists. Otherwise, the "mean slope-crossing" is taken into

account. If both are not found, the value is calculated as the mid-point of the boundaries. As a result, points on the lips and on the chin are coarsely extracted. The curves for the profile and the first and the second derivatives, lines for zero and the mean slope and their intersection points are depicted in Figure 4.

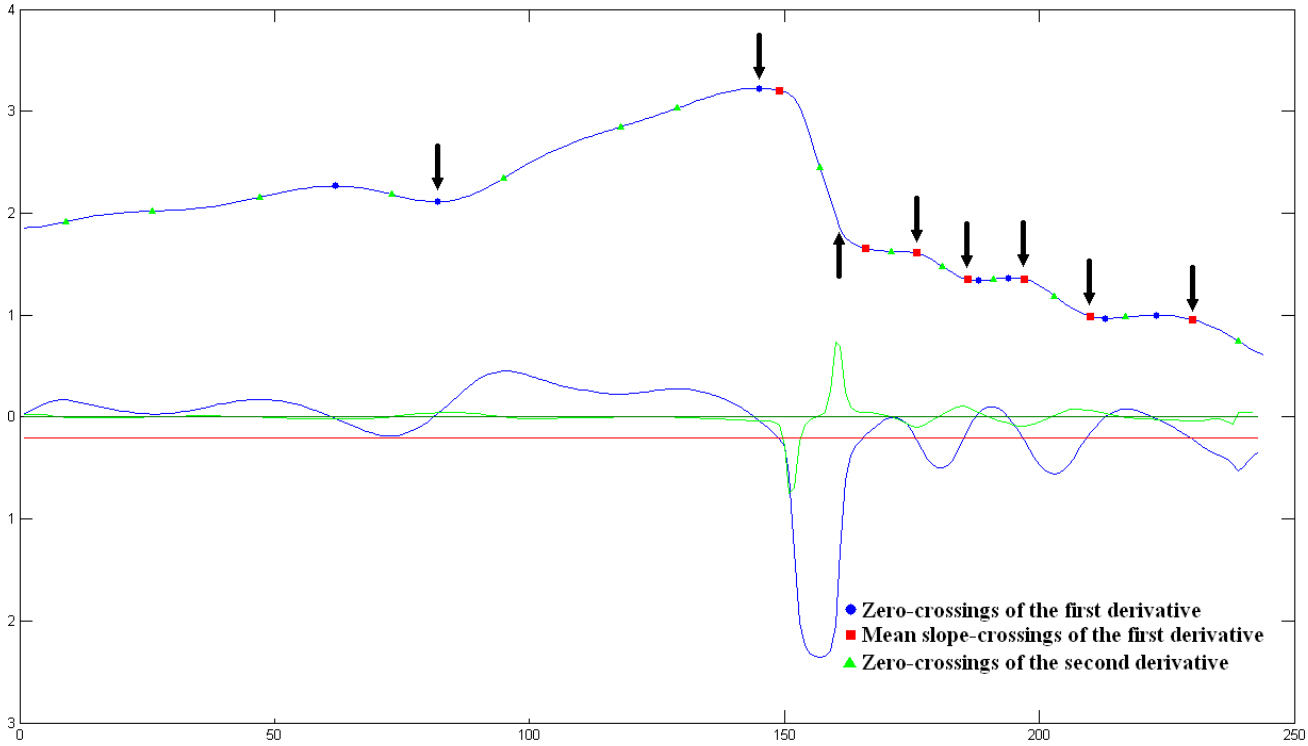

Figure 4: A sample profile curve and its first (blue) and second (green) derivative curves. The arrows show the eight detected interest points among the candidates

Now those landmarks are known, the face can be broken into more meaningful sub-images for locating or refining the points of interest.

3. EXTRACTION OF FACIAL INTEREST POINTS

After analyzing the vertical midline of the face, regions of interest for each eye and eyebrow, for nose and lips are extracted. The method for each part will be explained in detail in the following subsections.

3.1 Eyes

The 3D surface around the eyes tends noisy because of the reflective properties of the sclera and the pupil and the eyelashes. On the other hand, its texture carries highly descriptive information about the shape of the eye. For that reason, 2D data is utilized to detect the interest points around the eyes, namely the iris center, the inner and outer eye corners and the upper and the lower borders of the iris.

For this purpose, the method proposed in our previous work [9] is adopted. After applying an averaging filter with a rectangular kernel, and the noise and the horizontal edges are suppressed, the vertical edges are detected with Sobel operator and the edge map is cleaned with the help of morphological operators. Finally using the vertical edge image, similar to the previous step, the irises are detected by Hough transform.

For the eye corners detection, horizontal edges that belong to the eyelids are detected as described in [9] and two polynomials are fitted for lower and upper eyelids. The inner (near the nose bridge) and outer eye corners are determined as the intersection points of the two fitted polynomial.

After this step, the image is rotated one last time in the 2D image plane, if necessary, to horizontally align the two iris centers. An example is given in Figure 5.

Figure 5: Initial detection of iris circles in the upper half of the face, result of the detailed analysis for each eye and the re-rotated face to align iris centers

3.2 Nose

Contrary to the case with the eyes, nose region is extremely distinctive in surface but quite plain in texture. For this reason, we choose to proceed in 3D.

Initially, the yaw angle of the face is corrected in 3D. In order to achieve this correction, the horizontal curve passing through the previously found nose tip is examined. Ideally, the area under this curve should be equally partitioned by a vertical line passing through its maximum (assuming the nose is symmetrical) or at least the difference should be minimal. With this approach, the curve is iteratively rotated to minimize this difference between the two areas under the curve, divided by the newly calculated maximum point as the new nose tip. Once the angle is determined, the whole surface is rotated, so that a "more frontal" face is obtained.

After this adjustment, the minimum curvature is calculated for each point in the nose region. Then, edge detection is applied on the image in which the intensity is taken as the minimum curvature. . Those edges reveal the position of the interest points on both sides of the nose tip (Figure 6). Since they are not clearly defined, for the right and left upper edges of the nose, the points are assumed to be on the same horizontal line as the lower iris bounds and with a z value higher than ¼ of the nose tip.

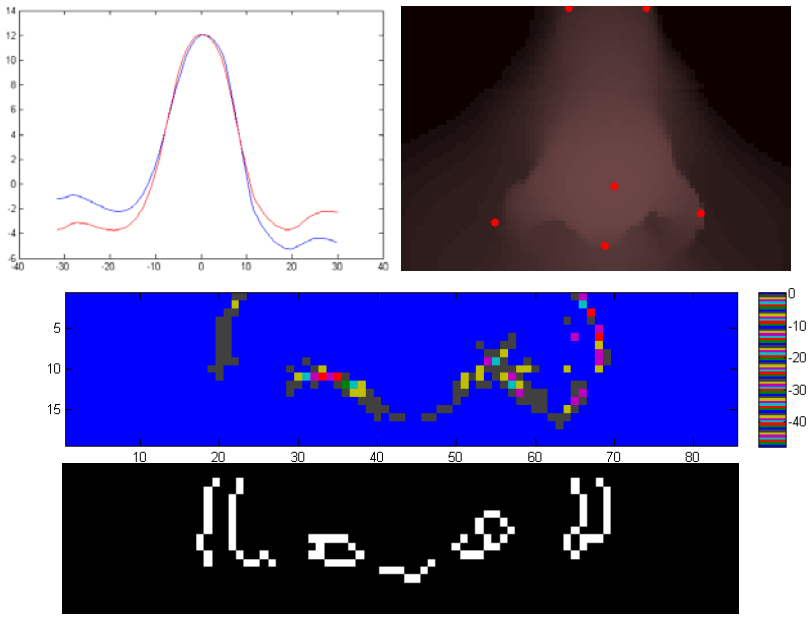

Figure 6: The horizontal profile of the nose tip before (blue) and after correction (red) is given along with the depth map of the nose region with detected points marked. The other two graphs show the minimum curvature and the corresponding edge map.

3.3 Eyebrows

In many studies to detect and track eyebrows [10, 11, 12, 15], template matching is utilized. The eyebrows are extracted with the help of edge map and according to a template. In a similar manner, in [13] the segmentation of the eyebrows involves fitting parametric models accurately based on the luminance gradient and in [14], a template for which the parameters are recovered by PCA analysis is utilized to represent the detailed shape information of eyebrows. On the other hand, there are also approaches [16, 17] where active contour model (snake) method is applied to extract the accurate eyebrow contour.

In our system, due to the fact that for eyebrow regions, the foreground and background are statistically different from each other but homogeneous within, region based (without edges) active contours approach is adopted. For this approach, initialization is a crucial step for accurate results. This problem is overcome by selecting the minimum in vertical projection of the smoothed grayscale images. For this purpose, histogram-equalized red channel of the eyebrow image is vertically projected (integral projection) and after the obtained curve is smoothed, an accumulation plot is created in which successive points with a negative derivative are counted. As a result, an approximate position for the eyebrow is found by taking the minimum value of the accumulation plot. The initial mask is created accordingly and the eyebrows are segmented based on the method proposed in [18]. After the contour is obtained, only the upper boundary is extracted and horizontal edge information, obtained by using Canny operator is added to it, in order to improve the robustness against false contour sections. Finally, a 3rd degree polynomial is fitted to remove the outliers and the first, the highest and the last points on the curve are taken as points of interest. Detailed example eyebrow segmentation is given in Figure 7.

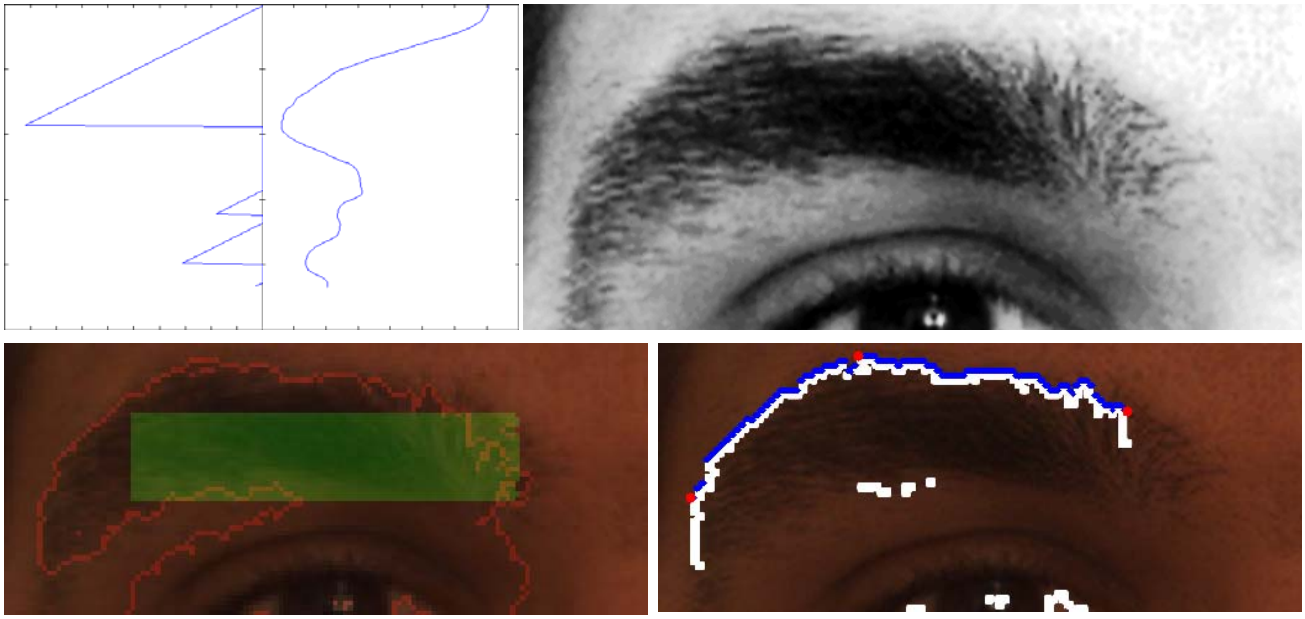

Figure 7: In the top row, vertical projection curve and its accumulation plot are given for the red channel of the eyebrow image whose histogram is equalized. In the bottom row, the initial mask (green) and the resultant segmentation is presented with the final contour merged with the edge map (white), the noise-free section after polynomial fitting (blue) and the points detected (red).

3.4 Lips

Although the lip region possesses similar properties with the eyebrow region, the color difference between skin and lips is not always as distinctive as the difference between the skin and the eyebrows. For this reason, we need a more appropriate approach than region based active contours. Numerous studies are proposed to extract the lip contour based on deformable [19] or active contour models [20, 21], working only with the 2D image. On the contrary, this is not the case with our system and thanks to the previous analysis on the vertical midline of the face; we have good estimates of three interest points on the lip.

Since we work on faces with neutral expressions, the mouth is assumed to be closed. A closed mouth always yields to a darker line between the two lips and based on this knowledge, the contact point of the lips is refined by applying a vertical projection analysis similar to that is suggested for eyebrows. Since that line should be represented with a nadir point in the projection, the row with a zero derivative and a minimum value is taken.

After obtaining the middle contact point for the lips, a narrow horizontal window is taken around that point to further analyze the dark line in between and to use that information to find the two endpoints of the lips. Horizontal edges are detected by iteratively decreasing the threshold until enough edge pixels are found and by horizontally projecting this edge map, the left and right corners of the lips are detected (Figure 8).

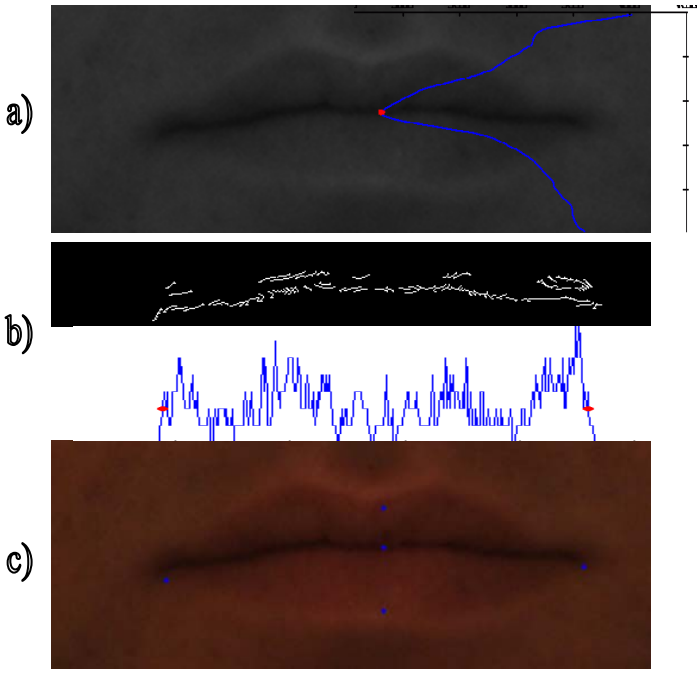

Figure 8: a) Grayscale image for lips and the plot for the horizontal projection. b) The edge map around the detected point and its vertical projection c) Resultant points

The upper and lower edges are not modified (they are located by the vertical profile analysis) unless there is a mistake due to the presence of moustache. In the case that a moustache is detected, the dark pixels in the grayscale image are masked out and the lip points' detection is executed in the remaining part. The moustache masking is achieved by intensity thresholding in the highly blurred grayscale image.

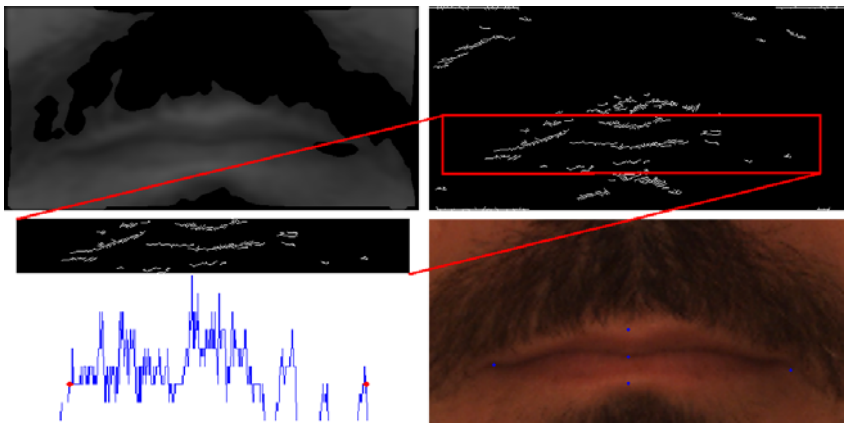

Figure 9: The obtained mask by thresholding removes the edges that the moustache creates and good estimates for the both corners of the lips are obtained.

4. TESTS AND RESULTS

In order to evaluate the performance of the proposed system, Bosphorus database [22] is utilized. This database contains 3D face scans and corresponding 2D color images, together with 2D and 3D coordinates of 24 labeled facial landmarks (Figure 10). Most of those landmarks coincide with the ones we detect. For the rest of them, the ground truth is created manually. Since the purpose of the proposed system is defined as to landmark neutral and frontal faces, the neutral set is utilized, which consists of frontal shots (2D+3D) of 105 subjects. The results are presented separately for each region in the following subsections.

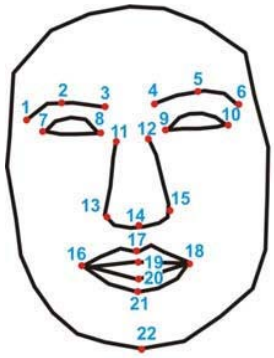

Labels of the 24 landmarks	
1. Outer left eye brow	2. Middle of the left eye brow
3. Inner left eye brow	4. Inner right eye brow
5. Middle of the right eye brow	6. Outer right eye brow
7. Outer left eye corner	8. Inner left eye corner
9. Inner right eye corner	10. Outer right eye corner
11. Nose saddle left	12. Nose saddle right
13. Left nose peak	14. Nose tip
15. Right nose peak	16. Left mouth corner
17. Upper lip outer middle	18. Right mouth corner
19. Upper lip inner middle	20. Lower lip inner middle
21. Lower lip outer middle	22. Chin middle

Figure 10: The manually labeled points in the Bosphorus database

4.1 Eyes

For the eye corners, manually noted landmarks are utilized. The error is taken to be the Euclidean distance between the detected and the manually labeled corner, after the images are scaled according to the distance between two iris centers where this distance is fixed to 60 pixels. For the threshold of 4 pixels error, 96.67% and 93.33% success rates are achieved for inner and outer eye corners, respectively. The results show that the algorithm performs better for the inner corners. This is because closer to the inner eye corners, the eyelid contours are more prominent than the ones around the outer eye corners. The error threshold vs. success rate graph is given in Figure 11.

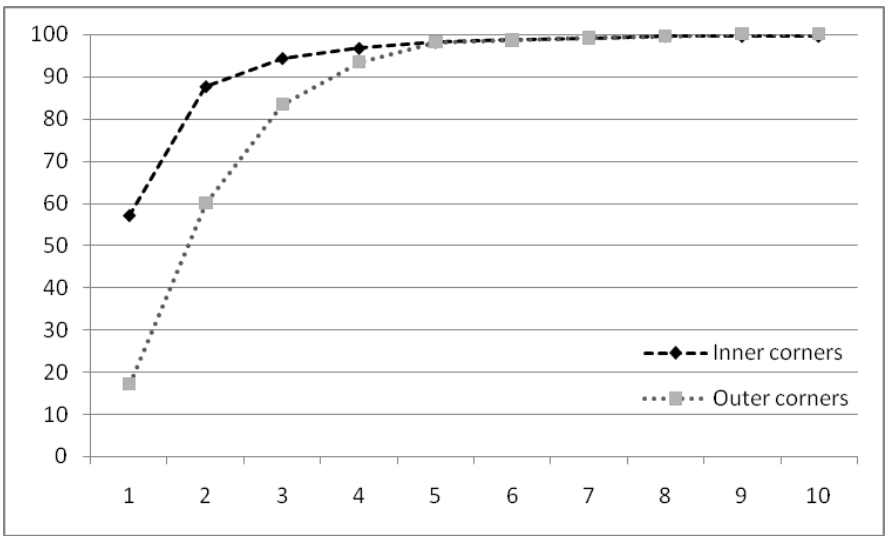

Figure 11: Eye corner detection rates for different error thresholds in size-normalized images.

On the other hand, since it is not very easy to determine the ground truth for iris center and the radius, visual examination is applied for iris extraction evaluation. The results are reported in Table 1.

Table 1: Success rates for iris localization compared with two other methods

Method	Threshold	Success rates
[23]	-	94.82%
[24]	-	94%
Our method	5 pixels	100%

4.2 Nose

Again, the ground truth files in the database are used for comparison for the interest points around the nose. The error is calculated as the Euclidean distance between the detected points and the ground truth, divided by the diagonal length of each 2D face image. In Table 2, the mean values and the standard deviations of the errors for 5 points (except the one at the bottom of the nose which is not included in the ground truth files) are given. Only the first 81 persons are taken into consideration since for the nose points some errors in the ground truth files (of the database) are detected for persons 82-105 (Figure 12).

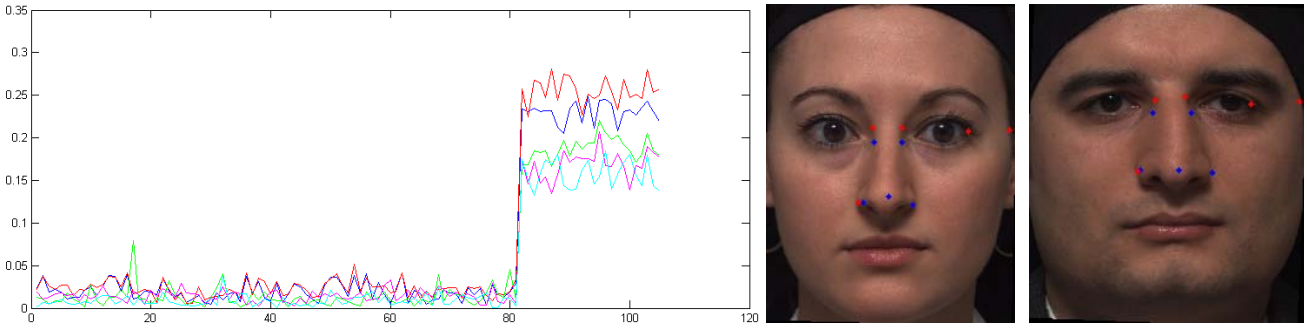

Figure 12: The error plot for 105 persons for 5 points on the nose. Between persons 82-105, there are errors in the ground truth files. Two samples are given in which detected points are shown in blue and the manually labeled points are shown in red.

Table 2: Mean and standard deviation values of the error for the points around the nose

Point (as labeled in Figure 10)	Error Mean	Error Std
Point #11	0.0194	0.0099
Point #12	0.0227	0.0094
Point #13	0.0126	0.0115
Point #14	0.0144	0.0066
Point #15	0.0088	0.0062

The first two points (nose saddle left and right) have the highest errors. When analyzed further, the reason is found to be in the definition of those interest points. Since in our approach those points are taken to be at the same horizontal line as the lower iris bound and with a z value higher than ¼ of the nose tip, the error represents the deviation of manual decisions from this definition.

For the point at the bottom of the nose, since its location is not always obvious in 2D images, the evaluation is done on the 3D vertical profile lines for each face. It is observed that 100% success rate is achieved with 2 pixels error threshold and for 94% of the faces, the bottom of the nose labeled impeccably.

4.3 Eyebrows

The difficulty in evaluating the detection of points around eyebrows stems from the ambiguity in their definition. To clarify the extent of the subjectivity, a test was conducted in which two persons are asked to manually label the points of interest and the differences between the detected and labeled points are analyzed together with the difference between two sets of labeled points (3 for each eyebrow: left, middle and right). In total, results for 210 eyebrows are compared. The success rates vs. error threshold plots for the three points are given separately in Figure 13, which include error between two labeled sets and between the detected points and the two sets of ground truth points.

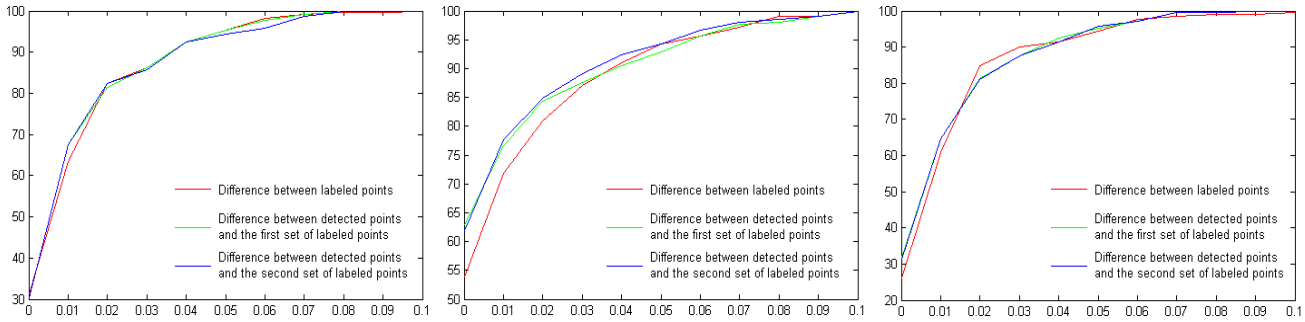

Figure 13: Rates vs. error threshold plots for the three points

As shown in the plots, the detection error follows a close path to the subjective error. The error axes in the graphs represent the Euclidean distance between points divided by the diagonal length of the cropped eyebrow image. For the final evaluation, the mean of the two labeled point sets are calculated as the ground truth. With this configuration, the obtained results are given in Table 3 for the thresholds of 4-6%.

Table 3: Detection rates for the left, middle and right points on the eyebrows when the success threshold is taken as 4-6%.

Points	%4	%5	%6
Left	%89.05	%93.33	%96.19
Middle	%91.43	%92.38	%94.29
Right	%88.57	%92.38	%95.71

4.4 Lips

The landmark files supplied with the database are used to evaluate the detection of interest points in the lip region. The mean and the standard deviation of the error for each of the 5 points are given in. Since the mouths are closed in the test set, the “upper lip inner middle” point is chosen as the middle point on the contact line of the lips.

Table 4: Error mean and its standard deviation for each lip point

Point (as labeled in Figure 10)	Error Mean	Error Std
#17	0.0128	0.0064
#19	0.0101	0.0038
#21	0.0144	0.0138
#16	0.0108	0.0083
#18	0.0135	0.0093

4.5 Chin

For the two points on the chin, the lower one is included in the database landmark files. For this point the mean error is found to be 0.0233 with a standard deviation of 0.0143. On the other hand, for the upper point, evaluation is done in the vertical profile plot in a similar manner as the bottom of the nose. It is seen that for 91.43% of the faces the point is detected within 3 pixels error threshold and 97.14% success rate is achieved when this threshold is taken as zero (perfectly detected). The errors are mostly due to the presence of the beard on the chin.

Table 5: Error mean and its standard deviation for the lower chin point

Point (as labeled in Figure 10)	Error Mean	Error Std
#22	0.0233	0.0143

Some example faces with detected and labeled points are given in Figure 14, together with an error plot for all persons and for all points labeled in the database.

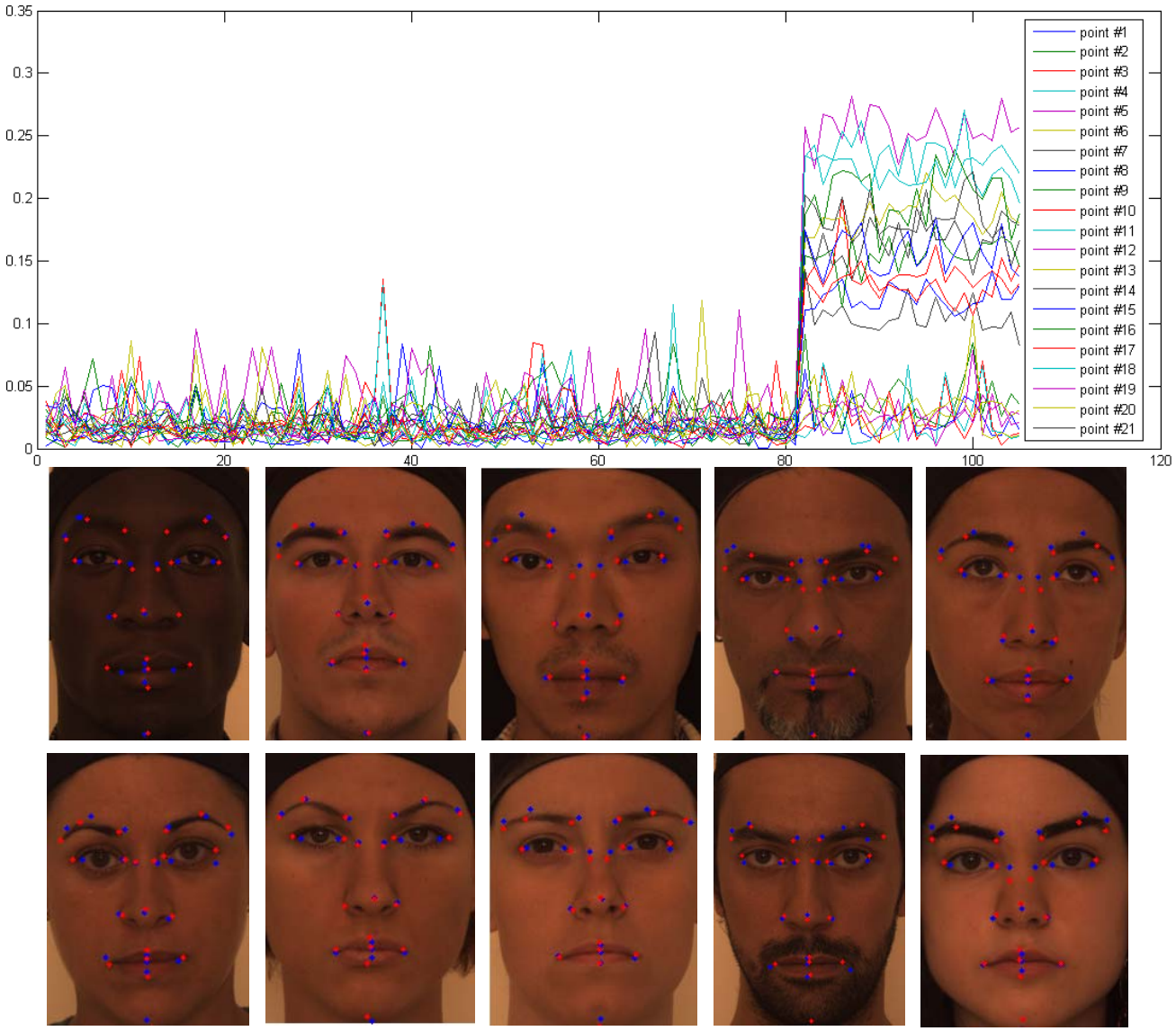

Figure 14: Error plot for all persons and for all points labeled in the database (for some points the labeled data in the database is obviously not reliable) and some examples of the resultant detected points (in blue) and the labeled points (in red)

5. CONCLUSION

In this paper, a method to find 29 interest points on frontal and neutral faces is presented, in which both 2D and 3D images of the faces are utilized. With the help of an extensive vertical profile analysis, the face is broken down to different sub-regions for eyes, eyebrows, nose and lips. Next, according to the region characteristics either 2D color images, either 3D scan data or both are analyzed in order to detect the points of interest. The algorithm is tested on the Bosphorus database that includes 105 subjects with registered 3D scans and color images. As a result, it is observed that accurate results can be achieved for each one of the points.

ACKNOWLEDGMENT

This research is supported by the ANR under the French project ANR-07-SESU-004 (FAR 3D: Face Analysis and Recognition using 3D).

REFERENCES

[1] Erdogmus, N., Dugelay, J. L., “Realistic and animatable face models for expression simulations in 3D”, SPIE, Electronic Imaging Conference on 3D Image Processing (3DIP) and Applications, January 17-21, 2010, San Jose, California

[2] Husken, M., Brauckmann, M., Gehlen, S., Von der Malsburg, C., “Strategies and Benefits of Fusion of 2D and 3D Face Recognition," IEEE Computer Society Conference on Computer Vision and Pattern Recognition – Workshops, CVPR Workshops. , pp.174-174, 25-25 June 2005

[3] Lu X., Jain, A.K., "Integrating Range and Texture Information for 3D Face Recognition," Seventh IEEE Workshops on Application of Computer Vision, vol.1, pp.156-163, 5-7 Jan. 2005

[4] Colbry, D., Stockman, G., Jain, A.K., "Detection of Anchor Points for 3D Face Verification," IEEE Computer Society Conference on Computer Vision and Pattern Recognition - Workshops, CVPR Workshops., pp.118-118, 25-25 June 2005

[5] Lu, X., Jain, A.K., “Multimodal facial feature extraction for automatic 3D face recognition,” Department of Computer Science, Michigan State University, East Lansing, Michigan, Tech. Rep. MSU-CSE-05-22, August 2005.

[6] Lu, X., Jain, A.K., "Automatic feature extraction for multiview 3D face recognition," Seventh International Conference on Automatic Face and Gesture Recognition, pp.585-590, 2-6 April 2006

[7] Boehnen, C., Russ, T., "A Fast Multi-Modal Approach to Facial Feature Detection," Seventh IEEE Workshops on Application of Computer Vision, vol.1, pp.135-142, 5-7 Jan. 2005

[8] Wang Y., Chua C. and Ho Y., “Facial Feature Detection and Face Recognition from 2D and 3D images”, Pattern Recognition Letters, 23:1191-1202, 2002

[9] Erdogmus, N., Dugelay, J. L., “An efficient iris and eye corners extraction method,” SSPR and SPR, Structural, Syntactic, and Statistical Pattern Recognition - Joint IAPR International Workshop, Cesme, Turkey, August, 2010

[10] Singh, N., "Face recognition by capturing eye illumination spot," Applied Imagery Pattern Recognition Workshop, Proceedings. 33rd , vol., no., pp. 153- 158, 13-15 Oct. 2004

[11] Hao Wang, Kongqiao Wang, , "Facial feature extraction and image-based face drawing," Signal Processing, 6th International Conference on , vol.1, no., pp. 699- 702 vol.1, 26-30 Aug. 2002

[12] Hara, F., Tanaka, K., Kobayashi, H., Tange, A., , "Automatic feature extraction of facial organs and contour," Robot and Human Communication. Proceedings., 6th IEEE International Workshop on , vol., no., pp.386-391, 29 Sep-1 Oct 1997

[13] Hammal, Z., Caplier, A., , "Eyes and eyebrows parametric models for automatic segmentation," Image Analysis and Interpretation, 6th IEEE Southwest Symposium on , vol., no., pp. 138- 141, 28-30 March 2004

[14] Kapoor, A., Picard, R.W., , "Real-time, fully automatic upper facial feature tracking," Automatic Face and Gesture Recognition, Proceedings. Fifth IEEE International Conference on , vol., no., pp.8-13, 20-21 May 2002

[15] Nikolaidis, A., Kotropoulos, C., Pitas, I., , "Facial feature extraction using adaptive Hough transform, template matching and active contour models," Digital Signal Processing Proceedings, 13th International Conference on , vol.2, no., pp.865-868 vol.2, 2-4 Jul 1997

[16] Chen, Q.R., Cham, W.K., Tsui, H.T., "A method for estimating and accurately extracting the eyebrow in human face image," International Conference on Image Processing, vol.3, no., pp. 793- 796 vol.3, 24-28 June 2002

[17] Huang C. L., Chen C. W., "Human facial feature extraction for face interpretation and recognition," 11th IAPR International Conference on Pattern Recognition, Conference B: Pattern Recognition Methodology and Systems, Proceedings, vol. 2, pp.204-207, 1992

[18] Chan T. and Vese L., “Active contours without edges”, IEEE Trans. Image Processing, 10(2):266–277, 2001.

[19] Liew, A.W.C., Leung, S.H., Lau, W.H., , "Lip contour extraction using a deformable model," Image Processing, Proceedings. 2000 International Conference on , vol.2, no., pp.255-258 vol.2, 10-13 Sept. 2000

[20] Ying Yang, Xiangdong Wang, Yueliang Qian, Shouxun Lin, , "Accurate and real-time lip contour extraction based on constrained contour growing," Joint Conferences on Pervasive Computing (JCPC), vol., no., pp.589-594, 3-5 Dec. 2009

[21] Xin Liu, Yiu-ming Cheung, Meng Li, Hailin Liu, , "A Lip Contour Extraction Method Using Localized Active Contour Model with Automatic Parameter Selection," 20th International Conference on Pattern Recognition (ICPR), , vol., no., pp.4332-4335, 23-26 Aug. 2010

[22] Savran A., Alyüz N., Dibeklioğlu H., Çeliktutan O., Gökberk B., Sankur B., Akarun L., "Bosphorus Database for 3D Face Analysis", The First COST 2101 Workshop on Biometrics and Identity Management, Roskilde University, Denmark, May 2008.
[23] Yepeng Guan, "Robust Eye Detection from Facial Image based on Multi-cue Facial Information," IEEE International Conference on Control and Automation, vol., no., pp.1775-1778, June 2007
[24] Kuo, P., Hannah, J., "An improved eye feature extraction algorithm based on deformable templates," IEEE International Conference on Image Processing, ICIP, vol.2, no., pp. II- 1206-9, 11-14 Sept. 2005